Article:
Eraslan, S., Gitman, I., Askes, H. et al. (2023) Effects of randomness and piezomagnetic coupling on the appearance of stop-bands in heterogeneous magnetorheological elastomers. Archive of Applied Mechanics, 93. pp. 3259-3273. ISSN: 0939-1533

https://doi.org/10.1007/s00419-023-02437-w

Archive of Applied Mechanics (2023) 93:3259–3273
https://doi.org/10.1007/s00419-023-02437-w

ORIGINAL

Sinan Eraslan · **Inna Gitman** · **Harm Askes** · **René de Borst**

Effects of randomness and piezomagnetic coupling on the appearance of stop-bands in heterogeneous magnetorheological elastomers

Received: 15 December 2022 / Accepted: 25 April 2023 / Published online: 12 May 2023

Abstract Phononic crystals (PCs) consist of a periodic arrangement of inclusions in a matrix material, and have garnered a great deal of interest owing to a phenomenon known as band gap frequencies in which particular frequency ranges are not able to propagate through the PCs. The aim of this work is to study the effects of magneto-elastic coupling and other parameters such as randomness in geometrical properties, volume fraction and size of inclusions on longitudinal wave propagation and, in particular, on the appearance of stop-band frequencies. The results indicate that the most important parameters deciding whether a frequency is in a stop-band or a pass-band are the randomness in geometrical properties and piezomagnetic coupling. It was observed that piezomagnetic coupling can lead to a widening of the first stop-band range for a periodic microstructure. Moreover, while randomness in particle size leads to a stop-band range and reduced wave transmission in the second pass region, randomness in particle position leads to removal of the pass band ranges compared to periodic structures. Additionally, the influence of piezomagnetic coupling becomes insignificant in fully random structures.

Keywords Magnetorheological elastomers · Wave propagation · Stop-band · Piezomagnetic coupling · Randomness

1 Introduction

It is well known that the behaviour of heterogeneous materials differs significantly from their homogeneous counterparts, specifically in dynamic problems. A considerable effort has been put on the study of elastic wave propagation in periodic composite materials by theoretical and experimental studies [1–6]. Composite

S. Eraslan (✉) · R. de Borst
Department of Mechanical Engineering, The University of Sheffield, Sheffield S1 3JD, UK
E-mail: seraslan1@sheffield.ac.uk

R. de Borst
E-mail: r.deborst@sheffield.ac.uk

I. Gitman · H. Askes
Faculty of Engineering Technology, The University of Twente, Twente, 7500 AE Enschede, The Netherlands
I. Gitman
E-mail: i.m.gitman@utwente.nl

H. Askes
E-mail: h.askes@utwente.nl

S. Eraslan · I. Gitman · H. Askes · R. de Borst
Department of Civil and Structural Engineering, The University of Sheffield, Sheffield S1 3JD, UK

materials with periodic arrangement of inclusions embedded in a matrix are known as phononic crystals (PCs) and they show a well-known phenomenon referred to as stop-band behaviour, where elastic wave propagation and vibrations are suppressed in certain frequency ranges [1,3,5,7–10]. Complete frequency gaps in PCs have potential for applications such as acoustic filters, reflectors, waveguides, switches and vibration isolation [4,9–12]. Controlling and tuning the characteristics (e.g. position and the width) of stop-bands and analysing the effective parameters influencing these properties are therefore important topics for investigation, allowing to create more effective designs or enhance the functionality of PCs. It is known that the stop-band attributes can be influenced by inclusion geometry, lattice pattern, volume fraction and elastic characteristics of the constituents [5,6,10,13].

Stimuli-responsive composite materials have also been extensively studied as they offer potential for superior features compared to conventional materials, in particular improved and controllable physical properties [6,12,14]. Therefore, these materials are attractive and promising candidates for stop-band tunability purposes. Specifically, PCs with piezoelectric or piezomagnetic constituents show some advantages compared to purely elastic PCs such as quick response, controllability and reversibility [15]. Bou Matar et al. [10] pointed out that large magnitudes of stimuli are needed to tune stop-band characteristics for electrorheological materials (or indeed temperature change) while magneto-elastic materials are very sensitive to external magnetic fields and their magnetic state. This feature makes magneto-elastic materials suitable candidates for contactless controllable PCs. They have already shown contactless tunability of stop-bands via the magnetic field dependent piezomagnetic material model for 2D PCs composed of Terfenol-D and an epoxy matrix [10]. It was concluded that introduction of magneto-elastic coupling can lead to some potentially advantageous effects on the band gap properties, such as an increase in bandwidth of the first stop-band range and the creation of a second stop-band range [10,12,16].

The influence of an external static magnetic field on band gaps of Lamb waves in PC slabs has been studied by Zhou et al. [11]. They concluded that the width of the first band gap can be changed significantly with a change in amplitude of the magnetic field, which can have potential applications in vibration isolation. Similarly, Ding et al. [9] have considered 1D magneto-elastic phononic crystals analysing and tuning longitudinal wave band gap properties. In addition to the static magnetic field, it was shown that filling fraction, pre-stress and thermal conditions can also influence band gap properties noticeably. Furthermore, elastic wave propagation in 2D magnetoelectroelastic materials has been investigated by Wang et al. [6,17] to understand the effects of lattice geometry and coupling effects on the bad gap characteristics. They demonstrated that the first band gap width is larger for triangular and square patterns as opposed to hexagonal geometries, and this difference increases with the filling ratio. On the other hand, piezoelectric and piezomagnetic effects have a significant influence (especially in high filling ratios) on the width of the higher band gaps.

Song et al. [5] demonstrated that geometrical and mechanical randomness also affect the stop-band frequencies in an elastic material. In particular, these authors showed that that randomness in the geometry causes much more significant changes on the stop-bands compared to mechanical randomness. Even for moderate perturbations in the geometry, the second pass band decreases dramatically, both in width and in transmission coefficient, and ultimately the second pass-band can be turned into a stop-band for a sufficiently high degree of geometric randomness.

The aim of this study is to analyse longitudinal wave propagation and stop-band behaviour in magneto-elastic composite materials and to investigate the combined influence of magneto-elastic coupling and randomness. The influence of the size and volume fraction of magnetic inclusions will be studied with and without magneto-elastic coupling. Randomness will be introduced in the magnetic inclusions' sizes and positions separately as well as simultaneously to analyse the effect of randomness in magneto-elastic composite material.

In Sect. 2, the finite element formulation will be described that has been used to simulate magneto-elastic wave propagation. The test setup and the algorithm of analysis will be given in Sect. 3. In Sect. 4, numerical results and discussions of different test material geometries are presented to study the effects of periodicity, randomness, particle size, volume fraction, and coupled versus decoupled behaviour. Finally, some closing remarks are presented in Sect. 5.

2 Continuum equations and discretisation aspects

Magnetostrictive materials exhibit non-linear material behaviour, but they can be described by linear piezomagnetic laws in a certain range of operation. This range can be obtained by considering only variations around

the initial magnetic bias and the mechanical pre-stress conditions [18]. The constitutive equations of a linear piezomagnetic medium in case of a static magnetic field (curl-free) are given as [8,19–22]

$$\boldsymbol{\sigma} = \mathbf{C}\boldsymbol{\varepsilon} - \mathbf{Q}\mathbf{H} \tag{1a}$$

$$\mathbf{B} = \mathbf{Q}^{\mathrm{T}}\boldsymbol{\varepsilon} + \boldsymbol{\mu}\mathbf{H} \tag{1b}$$

where $\boldsymbol{\sigma}$ and $\mathbf{B}$ are the stress and magnetic induction. $\mathbf{C}$, $\mathbf{Q}$ and $\boldsymbol{\mu}$ are the stiffness, piezomagnetic coupling and magnetic permeability matrices, respectively. $\boldsymbol{\varepsilon}$ and $\mathbf{H}$ are strain and magnetic field. The kinematic relations and equation of motion can be written as:

$$\boldsymbol{\varepsilon} = \mathbf{L}_{\mathrm{u}}\mathbf{u} \quad \text{and} \quad \mathbf{H} = -\mathbf{L}_{\varphi}\varphi \tag{2}$$

$$\mathbf{L}_{\mathrm{u}}^{\mathrm{T}}\boldsymbol{\sigma} = \rho\ddot{\mathbf{u}} \quad \text{and} \quad \mathbf{L}_{\varphi}^{\mathrm{T}}\mathbf{B} = 0 \tag{3}$$

Combining Eqs. (1–3) yields

$$\mathbf{L}_{\mathrm{u}}^{\mathrm{T}}\mathbf{C}\,\mathbf{L}_{\mathrm{u}}\mathbf{u} + \mathbf{L}_{\mathrm{u}}^{\mathrm{T}}\mathbf{Q}\,\mathbf{L}_{\varphi}\varphi = \rho\ddot{\boldsymbol{u}} \tag{4a}$$

$$\mathbf{L}_{\varphi}^{\mathrm{T}}\mathbf{Q}^{\mathrm{T}}\mathbf{L}_{\mathrm{u}}\mathbf{u} - \mathbf{L}_{\varphi}^{\mathrm{T}}\boldsymbol{\mu}\mathbf{L}_{\varphi}\varphi \;\; = 0 \tag{4b}$$

where $\mathbf{L}_{\varphi} = \boldsymbol{\nabla}$ and $\mathbf{L}_{\mathrm{u}}$ is the usual strain–displacement derivative operator, $\mathbf{u}$ is the displacement field, φ is the scalar magnetic potential, ρ is the mass density, and a superimposed dot denotes a time derivative.

To obtain the finite element formulation, the weak form of Eq. (4) can be written for domain $\boldsymbol{\Omega}$ and boundary $\boldsymbol{\Gamma}$ after integration by parts as follows:

$$\int_{\Omega} \mathbf{w}_{\mathrm{u}}^{\mathrm{T}}\rho\ddot{\mathbf{u}}\mathrm{d}\Omega + \int_{\Omega} (\mathbf{L}_{\mathrm{u}}\mathbf{w}_{\mathrm{u}})^{\mathrm{T}}\mathbf{C}\,\mathbf{L}_{\mathrm{u}}\mathbf{u}\mathrm{d}\Omega + \int_{\Omega} (\mathbf{L}_{\mathrm{u}}\mathbf{w}_{\mathrm{u}})^{\mathrm{T}}\mathbf{Q}\,\mathbf{L}_{\varphi}\varphi\mathrm{d}\Omega = \int_{\Gamma} \mathbf{w}_{\mathrm{u}}^{\mathrm{T}}\mathbf{t}_{\sigma}\mathrm{d}\Gamma \tag{5a}$$

$$\int_{\Omega} (\mathbf{L}_{\varphi}\mathrm{w}_{\varphi})^{\mathrm{T}}\mathbf{Q}^{\mathrm{T}}\mathbf{L}_{\mathrm{u}}\mathbf{u}\mathrm{d}\Omega - \int_{\Omega} (\mathbf{L}_{\varphi}\mathrm{w}_{\varphi})^{\mathrm{T}}\boldsymbol{\mu}\mathbf{L}_{\varphi}\varphi\mathrm{d}\Omega = \int_{\Gamma} \mathrm{w}_{\varphi}^{\mathrm{T}}\mathbf{t}_{\mathrm{B}}\mathrm{d}\Gamma \tag{5b}$$

where $\mathbf{w}_{\mathrm{u}}$ and w_{φ} are the test functions, $\mathbf{t}_{\sigma}$ are the mechanical boundary tractions, and $\mathbf{t}_{\mathrm{B}}$ is the magnetic traction on the boundary. Thus, the following system of equations is obtained:

$$\begin{bmatrix} \mathbf{M} & \mathbf{0} \\ \mathbf{0} & \mathbf{0} \end{bmatrix} \begin{bmatrix} \ddot{\mathbf{d}} \\ \mathbf{0} \end{bmatrix} + \begin{bmatrix} \mathbf{K}_{\mathbf{uu}} & \mathbf{K}_{\mathbf{u}\varphi} \\ \mathbf{K}_{\varphi\mathbf{u}} & -\mathbf{K}_{\varphi\varphi} \end{bmatrix} \begin{bmatrix} \mathbf{d} \\ \boldsymbol{\Psi} \end{bmatrix} = \begin{bmatrix} \mathbf{F} \\ \boldsymbol{\Phi} \end{bmatrix} \tag{6}$$

where $\mathbf{d}$ and $\boldsymbol{\Psi}$ are nodal displacement and nodal scalar magnetic potential vectors via $\mathbf{u} = \mathbf{N}_{\mathrm{u}}\mathbf{d}$, $\ddot{\boldsymbol{u}} = \mathbf{N}_{\mathrm{u}}\ddot{\boldsymbol{d}}$ and $\varphi = \mathbf{N}_{\varphi}\boldsymbol{\Psi}$. Moreover, $\mathbf{F}$ and $\boldsymbol{\Phi}$ are nodal mechanical force and nodal magnetic flux vectors. Lastly, stiffness and mass matrices are given by

$$\mathbf{M} = \int_{\boldsymbol{\Omega}} \rho\mathbf{N}_{\mathrm{u}}^{\mathrm{T}}\mathbf{N}_{\mathrm{u}}\mathrm{d}\Omega, \qquad \mathbf{K}_{\mathrm{uu}} = \int_{\Omega} \mathbf{B}_{\mathrm{u}}^{\mathrm{T}}\mathbf{C}\mathbf{B}_{\mathrm{u}}\mathrm{d}\Omega\mathbf{K}_{\mathrm{u}\varphi} = \int_{\boldsymbol{\Omega}} \mathbf{B}_{\mathrm{u}}^{\mathrm{T}}\mathbf{Q}\mathbf{B}_{\varphi}\mathrm{d}\Omega,$$

$$\mathbf{K}_{\varphi\mathrm{u}} = \int_{\boldsymbol{\Omega}} \mathbf{B}_{\varphi}^{\mathrm{T}}\mathbf{Q}^{\mathrm{T}}\mathbf{B}_{\mathrm{u}}\Omega\mathbf{K}_{\varphi\varphi} = \int_{\boldsymbol{\Omega}} \mathbf{B}_{\varphi}^{\mathrm{T}}\boldsymbol{\mu}\mathbf{B}_{\varphi}\mathrm{d}\Omega \tag{7}$$

with $\mathbf{B}_{\mathrm{u}} = \mathbf{L}_{\mathrm{u}}\mathbf{N}_{\mathrm{u}}$, $\mathbf{B}_{\varphi} = \mathbf{L}_{\varphi}\mathbf{N}_{\varphi}$. The matrices $\mathbf{N}_{\mathrm{u}}$ and $\mathbf{N}_{\varphi}$ contain the relevant shape functions of linear triangular finite elements.

In order to integrate the equations of motion in time, the constant average acceleration variant of the Newmark method has been used.

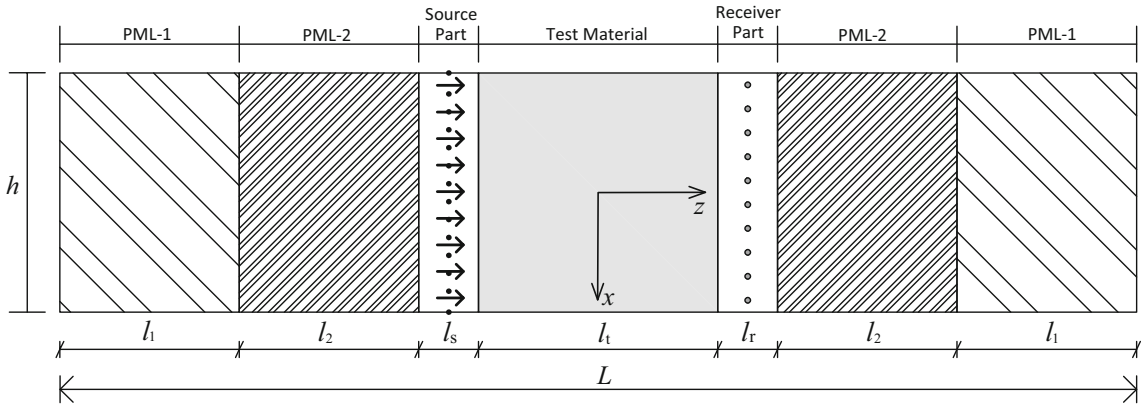

Fig. 1 Numerical model of simulation

Table 1 Size of the parts in the test setup (mm)

	Test material	Source/receiver	PML-1/PML-2
Length (l)	2	0.5	1.5
Height (h)	2	2	2

3 Numerical test setup

The test setup has been constructed as given in Fig. 1. The test material (MRE) consists of polymer matrix and piezomagnetic particles. It is known that reflections either from the interface between the parts or from the ends of the geometry can significantly affect the results in a wave propagation analysis. So-called perfectly matched layers (PMLs) are often used in numerical simulations to absorb the waves, so that unwanted reflections can be avoided [5]. Additionally, it was pointed out that spurious reflections can pollute the results, if the difference in compressional wave speeds between the PMLs and source/receiver parts is too large [5]. Therefore, two PMLs have been created in the test setup to reduce this numerical noise (Table 1).

The test material (MRE) has been placed between PMLs and artificial source/receiver regions to simulate the longitudinal waves propagating in the test material along the z axis. Here, the superscripts 1, 2, s and r represent the first PML, the second PML, source and receiver regions respectively. The acoustic impedance of PMLs and source/receiver parts should be identical to provide a smooth transition between the various parts and low compressional wave speeds in the PMLs [5]. Therefore, the material properties have been taken as

$$\begin{aligned} &\rho^{\mathrm{s}} = \rho^{\mathrm{r}} \quad \rho^{2} = 10\rho^{\mathrm{s}} \quad \rho^{1} = 50\rho^{\mathrm{s}} \\ &\mathbf{C}^{\mathrm{s}} = \mathbf{C}^{\mathrm{r}} \quad \mathbf{C}^{2} = 0.1\mathbf{C}^{\mathrm{s}} \quad \mathbf{C}^{1} = 0.02\mathbf{C}^{\mathrm{s}} \end{aligned} \tag{8}$$

where ρ is the mass density and $\mathbf{C}$ is the stiffness matrix. Thus, the compressional matching impedance has been achieved via $\sqrt{\rho^{\mathrm{s}} C^{\mathrm{s}}_{33}} = \sqrt{\rho^{\mathrm{r}} C^{\mathrm{r}}_{33}} = \sqrt{\rho^{1} C^{1}_{33}} = \sqrt{\rho^{2} C^{2}_{33}}$, where C_{33} is the stiffness in direction of longitudinal wave propagation along the z axis. Furthermore, the compressional wave speed in the various parts follows from

$$v^{\mathrm{s}}_{\mathrm{comp.}} = v^{\mathrm{r}}_{\mathrm{comp.}}, v^{2}_{\mathrm{comp.}} = \sqrt{\frac{C^{2}_{33}}{\rho_2}} = 0.1 v^{\mathrm{s}}_{\mathrm{comp.}} \, v^{1}_{\mathrm{comp.}} = \sqrt{\frac{C^{1}_{33}}{\rho^{1}}} = 0.02 v^{\mathrm{s}}_{\mathrm{comp.}} \tag{9}$$

The process to identify stop-bands and pass-bands can be summarized as follows:

1. Mechanical boundary conditions have been prescribed as $u_z\left(-\frac{L}{2}\right) = u_z\left(\frac{L}{2}\right) = 0, u_x\left(-\frac{L}{2}\right) = u_x\left(\frac{L}{2}\right) = 0$ and $u_x\left(-\frac{h}{2}\right) = u_x\left(\frac{h}{2}\right) = 0$ where u_x and u_z are horizontal and vertical displacements. Magnetic boundary conditions have been set up by defining scalar magnetic potentials Ψ^{s} and Ψ^{r} on the nodes of source and receiver lines (at the middle of the source/receiver parts, see Fig. 1) to model a static external magnetic field $\mathbf{H}_{\mathrm{o}}$ affecting the test material. Scalar magnetic potentials on the receiver and source nodes have been

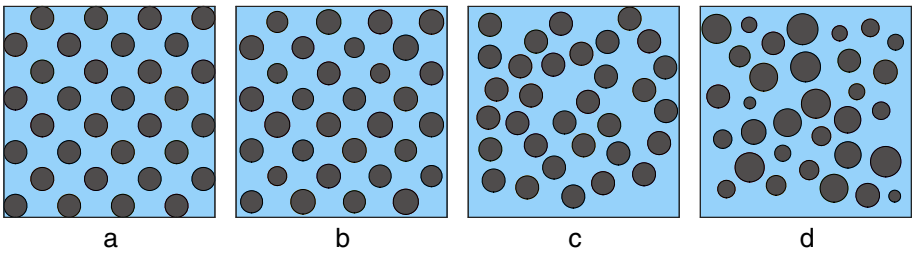

Fig. 2 Example of test materials. Periodic (**a**), randomness in particle size (**b**), position (**c**) and both (**d**). ($V_f = 30\%$)

set to be −6.25 A and 6.25 A, respectively. These potentials create 5 kA/m of external magnetic field $\mathbf{H}_o$ between source and receiver lines that corresponds to a small variation around bias field [18]. Lastly, initial conditions at $t = 0$ have been defined as $\mathbf{v} = 0$ and $\mathbf{u} = 0$ where $\mathbf{v}$ is the nodal velocity vector.

2. A continuous harmonic longitudinal sine wave is activated at the source line by applying nodal forces $F_g = A_g \sin(\omega t)$ where A_g is the amplitude, ω is the angular frequency and t is time. This longitudinal wave propagates in the positive z direction through the test material (MRE) and the displacements on the receiver line are recorded.
3. For each frequency, two simulations are set: one with a heterogeneous test material, and one with the equivalent homogeneous test material. In the homogenous setup, material properties of the test material are averaged from magnetic particle and polymer matrix according to the rule of mixtures. In the heterogeneous setup, constituents have their individual material properties. The material properties of the source and receiver parts are assigned to be the averaged properties in both simulations.
4. To have the amplitudes of propagated incident wave for both homogeneous (A_h) and heterogeneous (A_c) setup, a Fourier transform is applied to the recorded displacements at the end of each simulation. It is known that wave propagation is non-dispersive in homogeneous materials, and each individual harmonic travels with the same velocity. However, the wave propagation will show a dispersive behaviour in case of heterogeneous materials, and an inability of certain harmonic components to propagate may occur. The amplitude variance between the homogeneous and heterogeneous configurations will be used to define the transmission coefficient. Displacements are recorded on ten equally spaced nodes (recording points) at the receiver line during the simulation. Finally, a transmission coefficient is defined as

$$T = \frac{A_c}{A_h} \tag{10}$$

In this study, it was assumed that if the transmission coefficient is less than 10%, the relevant harmonic component can be considered as "stopped". This process has been followed for a range of frequencies to determine the stop-band frequency ranges. By varying microstructural properties of the test material and applying or switching off magnetic field, the effects of microstructure and magneto-elastic coupling can be measured and assessed in a systematic manner.

4 Results and discussion of numerical test

In the numerical analysis, material properties of magnetostrictive Terfenol-D particles and polymer matrix material have been adopted as given in Table 2. The polymer matrix has been modelled to be a non-magnetisable material. To represent the non-magnetisable polymer, piezomagnetic constants of the matrix have been assumed as zero, and the magnetic permeability of the matrix has been taken as the magnetic permeability of air. Damping of the constituents have been assumed as zero to simplify the analysis [23], and volume fractions of particles V_f have been chosen as 30 and 45% (for different tests). A continuous harmonic force function has been applied with an amplitude (A_g) of 1 Newton during the simulation time which has been set to be equal 30 periods of the wave to ensure that sufficient periods have propagated and been recorded. To describe the wave propagation accurately, approximately 6 finite elements per wavelength were used in the test material. The studied frequency range has been set to be 0.5–7.0 MHz.

As mentioned above, the effects of piezomagnetic coupling and microstructure of the MRE have been investigated in this study. To study the coupling effect, the piezomagnetic coupling properties of the particles have been assigned as zero and non-zero (see Table 2) to simulate decoupled and coupled physics. Moreover,

Table 2 Material properties

	Coupled		Decoupled	
	Terfenol-D[a]	Polymer[b]	Terfenol-D[a]	Polymer[b]
C_{11}	27	7.8	27	7.8
C_{13}	11.8	4.8	11.8	4.8
C_{33}	31.4	7.8	31.4	7.8
C_{55}	4.2	1.6	4.2	1.6
q_{31}	-15.2	0	0	0
q_{33}	217	0	0	0
q_{15}	68	0	0	0
μ_{11}	9	μ_0	μ_0	μ_0
μ_{33}	1.68	μ_0	μ_0	μ_0
ρ	9250	1150	9250	1150

C_{ij} in GPa, q_{ij} in N/Am, μ_{ij} in 10^{-6}N/A^2, ρ in kg/m^3
[a,b]Adopted from [18,24], respectively

the magnitude of the external magnetic field $\mathbf{H}_{\text{o}}$ has been set to be 0 kA/m for the decoupled case, and 5 kA/m for the coupled case in the z direction.

In the evaluation of the microstructure, attributing to our earlier studies [5,23,25], periodic and random particle distributions have been created for the test material. To this end, alongside periodic material (a), randomness has been introduced in terms of particle size only (b), particle position only (c), and both size and position simultaneously (d) as depicted qualitatively in Fig. 2.

4.1 Periodic microstructure

We start our analysis with a periodic test material (Fig. 2a), which will serve as a benchmark for all subsequent tests.

4.1.1 Influence of magneto-elastic coupling

In this first study, the influence of piezomagnetic coupling on the wave propagation in periodic material has been evaluated. The transmission coefficients on the recording points have been calculated for each frequency, and an averaged transmission coefficient $\overline{T}$ has been determined for each frequency as the mean of the ten T_i, recorded in the ten receiver points to visualise and compare results more quantitatively as shown in Fig. 3. It must be noted that these average values $\overline{T}$ represent the change in the trend of transmission coefficients along the frequency range, and it should not be used as the only result to assess the propagation of the wave in the test material. However, since transmission coefficients T_{i} at the stop-band frequencies are similar, the averaged value can represent the wave propagation and transmission coefficients on the recording line. Fig. 3 shows stop-band frequencies range of 2.1–2.6 MHz for the case of pure elasticity (or decoupled with absence of magnetic field). When the piezomagnetic coupling terms are introduced (or coupled with presence of magnetic field), the width of the first stop-band increases to 2.1–3.1 MHz, presenting a slightly enlarged stop-band characteristic for the test material.

4.1.2 Influence of volume fraction of inclusions

It is known that the volume fraction of the inclusions is an influential parameter on the static and dynamic behaviour of MREs [6,10,12,26]. It was previously reported that a higher volume fraction of magnetic particles can lead to increased band width and transition of the stop-band frequencies. Therefore, it is worth investigating the effect of the volume fraction. To study this effect, another periodic test material has been created by increasing the volume fraction to 45% as seen in Fig. 4.

As seen in the averaged transmission coefficient results (see Fig. 5), an increase in volume fraction affects the wave propagation characteristics noticeably. Increasing the particle volume fraction moves the frequency ranges 3.5–4.0 MHz and 6.5–7.0 MHz into stop bands for the decoupled physics case. For the coupled physics case, increasing the particle volume fraction leads to a considerably wider first stop band of 2.0–5.5 MHz.

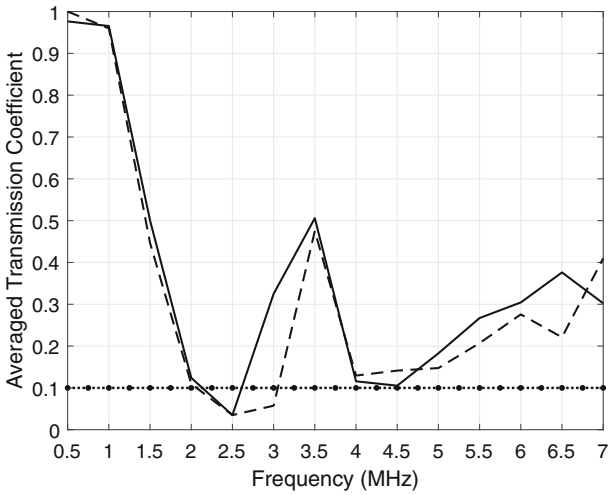

Fig. 3 The average transmission coefficient $\overline{T}$ and effect of magneto-elastic coupling on the stop-band frequencies in periodic microstructure. Decoupled (solid), coupled (dashed) of magnetic field cases. Dashed-dotted line presents 10% cut-off indicating stop-band

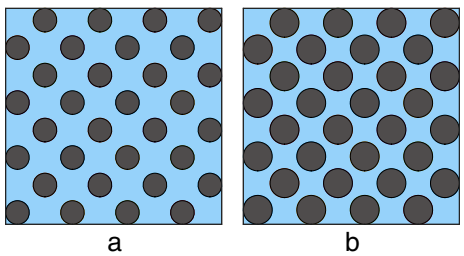

Fig. 4 Increased volume fraction for periodic test material: $V_f = 30\%$ (**a**), $V_f = 45\%$ (**b**)

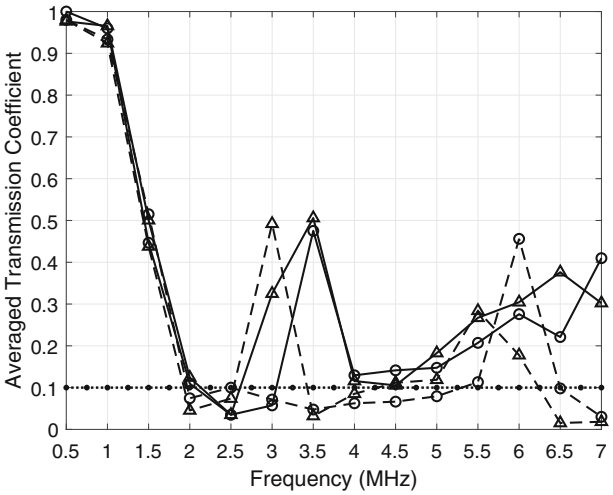

Fig. 5 The average transmission coefficient $\overline{T}$ and the effect of volume fraction on the wave propagation in coupled (circle)/decoupled (triangle) cases. $V_f = 30\%$ (solid) and $V_f = 45\%$ (dashed)

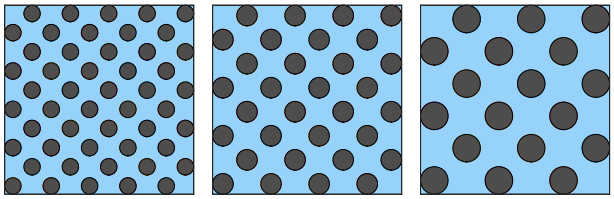

Fig. 6 Different particle sizes: smaller (**a**), original (**b**), larger (**c**) ($V_f = 30\%$)

4.1.3 Influence of particle sizes

The particle size is another geometric parameter influencing the wave propagation. To study this parameter, three different (but each uniform) size configurations have been created (see Fig. 6). Figure 7 presents the averaged transmission coefficient results for smaller (dashed), original (solid) and larger (dash-dotted) particle size configurations. It can be seen that with decreasing particles sizes, the first stop-band frequency moves to higher values and the first stop-band widens for both coupled and decoupled cases. It is also useful to note, that coupled cases for each size configuration present increased first stop-band widths compared to their decoupled counterparts.

4.2 Random microstructure

Next, random microstructural configurations are considered. Geometrical randomness has been introduced in terms of particle size, particle position, and both (see Fig. 2). A volume fraction of inclusions of 30% has been assumed for all random microstructures. To investigate particle size randomness, a uniform particle diameter distribution of 110–240 μm is assumed to create random sizes for particles in a periodic pattern (Fig. 8).

The average transmission coefficients in Fig. 9 show that randomness added to particles sizes leads to increased first stop-band width for both the decoupled and coupled physics cases. Besides, different realisations of the particles size randomness present similar results to a certain degree in the first stop-band and second pass-band regions. However, there are noticeable differences between the realisations and periodic case with identical particles.

For the next test, identical particles with random positions have been used for position randomness by using a MATLAB code developed in-house (Fig. 10).

Figure 11 depicts that randomness added to particles positions has a much more significant influence on the results by removing almost all the second pass-band frequencies and turning them into a stop-band in both coupled and decoupled cases. It can also be noted that randomness in positions leads to more dispersive wave propagation in the test material, and thus transmission coefficients in pass-band frequencies are generally significantly lower compared to the periodic benchmark case while randomness in particle size still maintains a level of geometric periodicity and, thus, it still provides distinct stop and pass-band regions.

Next, randomness has been introduced to both particle sizes and position simultaneously. Three different *fully* random test materials have been created as seen in Fig. 12. The distributions of the average transmission coefficients in Fig. 13 show results of random realisations and present the difference with the periodic test material. As seen, all three random realisations present very similar behaviour by removing the second pass-band compared to periodic arrangement. This difference can also be seen in Fig. 14 via 3D plots of the transmission coefficients T_{i}. Furthermore, note that the difference between the coupled and decoupled cases has become negligible in a fully random test material (see Fig. 14b).

Note that the results of random test materials in Fig. 13 present similar wave propagation characteristics compared to the case of the randomness added to the position only (see Fig. 11). However, the transmission coefficients in the second pass-band have been reduced slightly more than the position randomness, and the second pass-band has been turned into stopped frequencies.

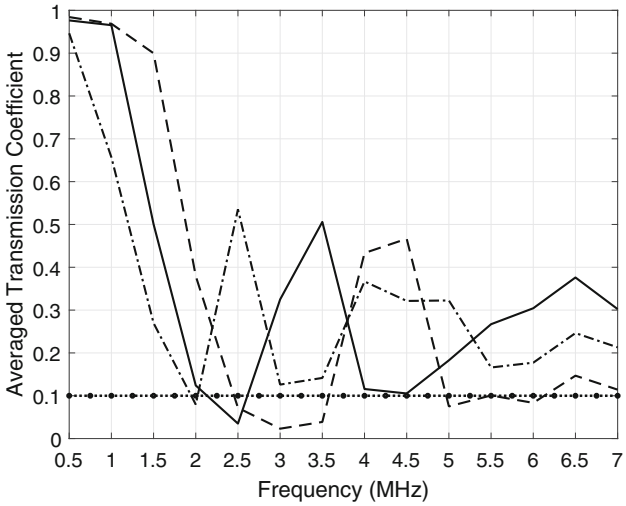

(a) Decoupled

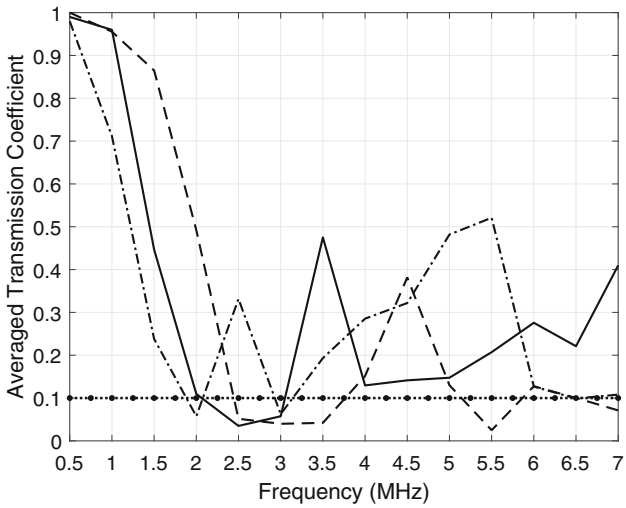

(b) Coupled

Fig. 7 The average transmission coefficient $\overline{T}$ and the effect of particle size on the wave propagation in coupled/decoupled cases. Particle sizes: smaller (dashed), original (solid), and larger (dash-dotted)

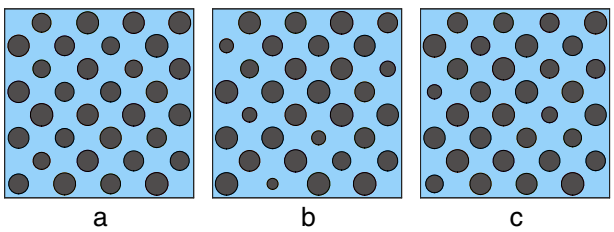

Fig. 8 Randomness added to particles sizes. Three different realisations a, b and c from left to right. ($V_f = 30\%$)

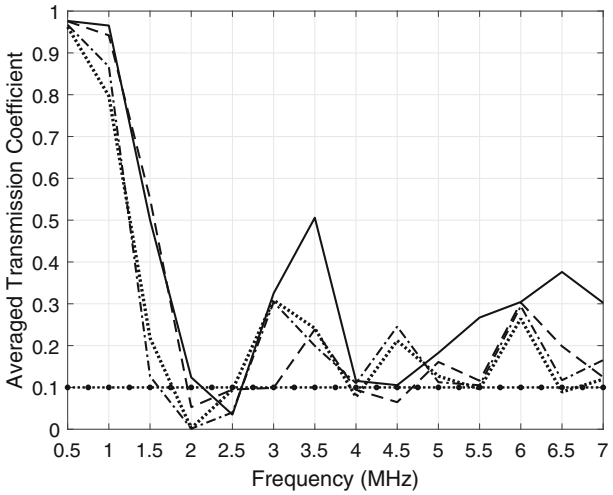

(a) Decoupled

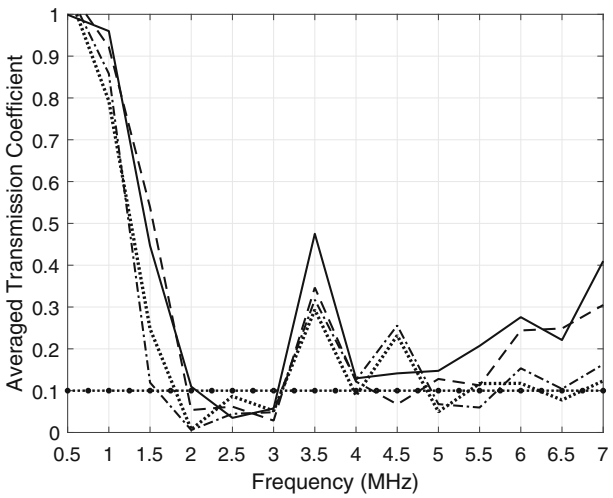

(b) Coupled

Fig. 9 The average transmission coefficient $\overline{T}$ in case of randomness in particle size. Periodic (solid), realisation—a (dashed), realisation—b (dotted), realisation—c (dash-dotted)

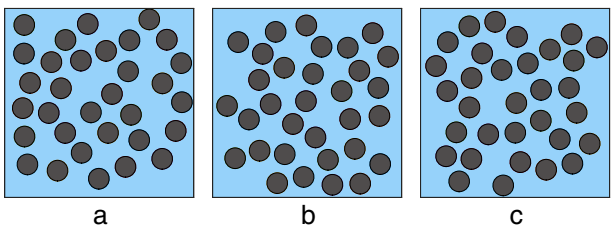

Fig. 10 Randomness added to particles position. Three different realisations a, b and c from left to right. ($V_f = 30\%$)

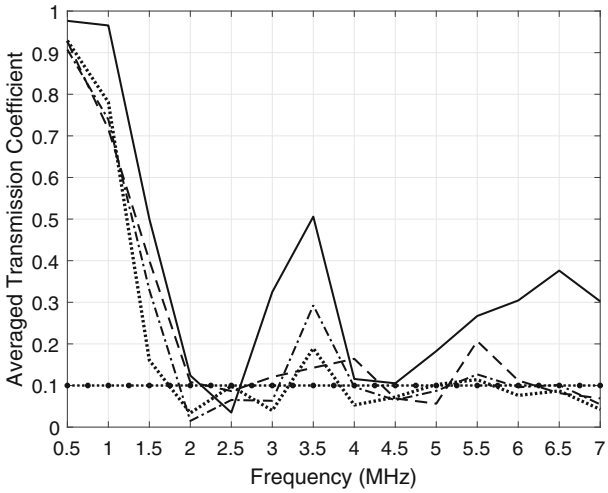

(a) Decoupled

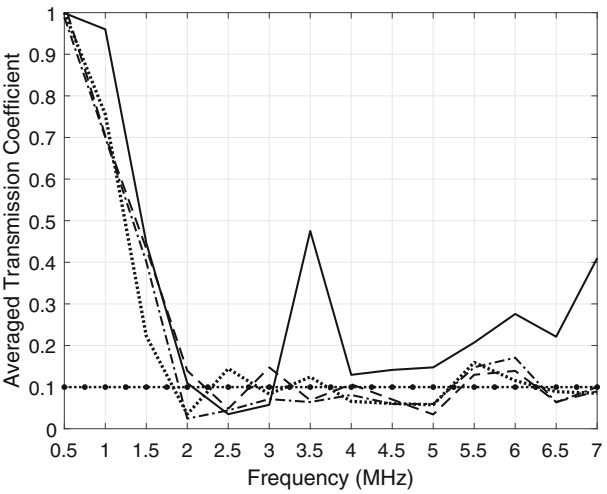

(b) Coupled

Fig. 11 The average transmission coefficient $\overline{T}$ in case of randomness in particle position. Periodic (solid), realisation—a (dashed), realisation—b (dotted), realisation—c (dash-dotted)

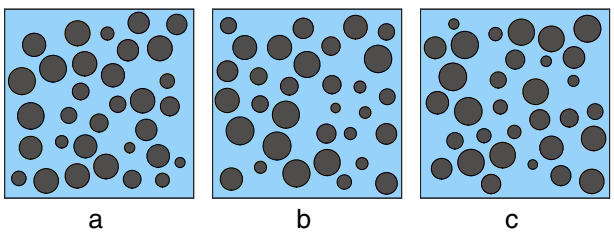

Fig. 12 Randomness added to particles sizes and positions simultaneously. Three different realisations a, b and c from left to right ($V_f = 30\%$)

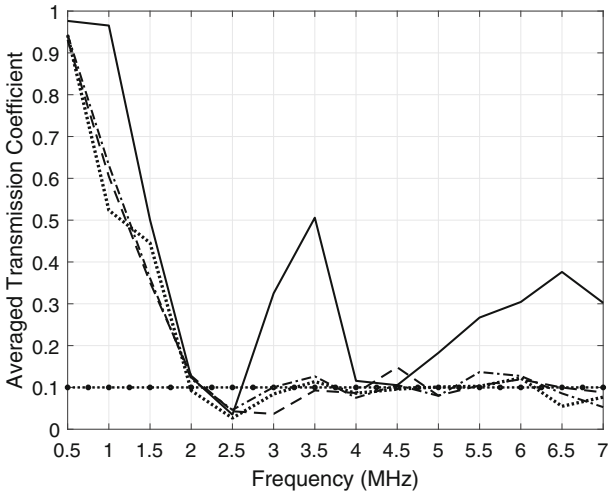

(a) Decoupled

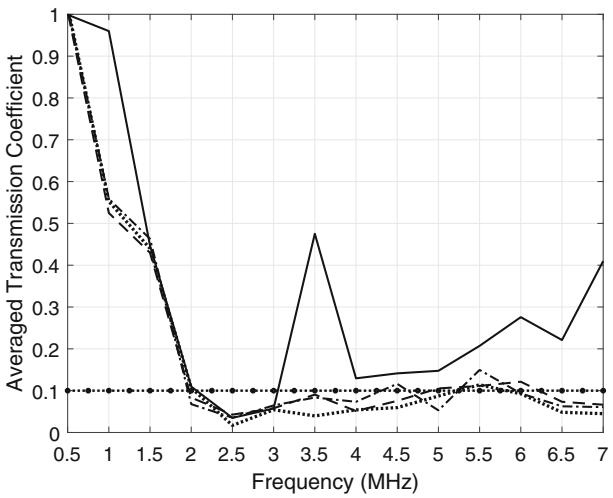

(b) Coupled

Fig. 13 The average transmission coefficient $\overline{T}$ in case of fully random material realisations and periodic material. Periodic (solid), realisation—a (dashed), realisation—b (dotted), realisation—c (dash-dotted)

5 Conclusions

In this study, the effects of magneto-elastic coupling and variations in geometry of microstructures on the longitudinal wave propagation and stop-bands have been studied for a magnetorheological elastomer. Longitudinal sine waves have been created during the simulation time in the source region and these waves have been recorded in the receiver region after having propagated through the test material.

In a material with a periodic structure, it was seen that the particle size and volume fraction are important parameters in the stop-band frequencies. For the same volume fraction, decreasing the particle size has resulted in a wider first stop-band gap and a shift of the first stop-band frequency to a higher frequency value. Furthermore, a distinct difference in the first band gap has been observed between coupled and decoupled considerations for these tests. When magneto-elastic coupling was introduced to the system, test geometries exhibited a wider band gap. Moreover, the volume fraction of inclusions also has a notable effect on the characteristics: it was observed that pass-band frequencies can be transferred into the stop-band in case of higher volume fractions. The difference between coupled and decoupled formulations has also been significantly increased for higher volume fractions resulting in a possible second stop-band.

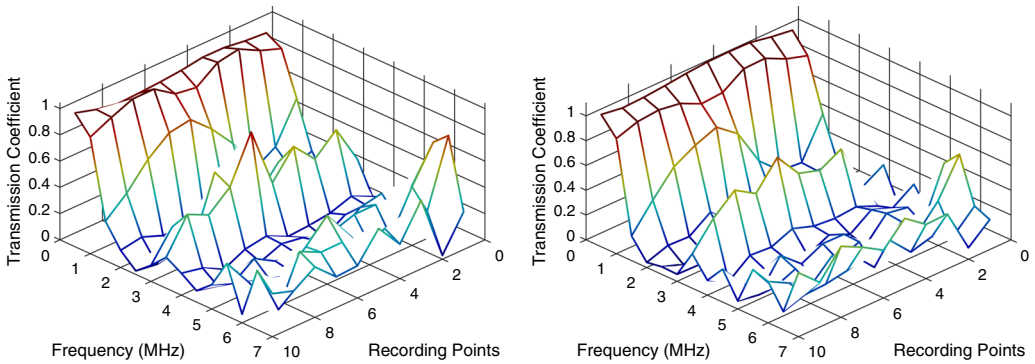

(a) Periodic structure. Decoupled (left) and coupled (right).

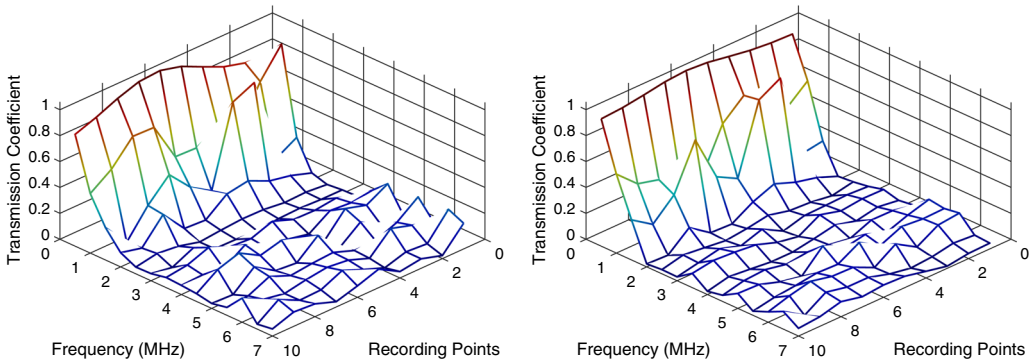

(b) Randomness added to both particles sizes and positions simultaneously. Decoupled (left) and coupled (right).

Fig. 14 Transmission coefficients T_i in periodic and fully random test materials

Next, materials with geometrically random microstructure have been analysed. It was observed that randomness added to particle size reduces the transmission coefficient in the second pass range although the first band gap remained similar to that of periodic materials. However, introduction of randomness to particle position leads to the complete removal of the pass-band ranges in both coupled and decoupled cases. Lastly, fully random test materials with randomness added to both sizes and positions have been investigated. Full randomness exhibited stop-band characteristics similar to those of randomness added to position only. It was observed that the pass-band ranges tend to be removed in case of full randomness similar to positions randomness. Therefore, it can be concluded that particle position randomness is much more significant than particle size randomness in wave propagation behaviour. Interestingly, the effects of magneto-elastic coupling compared to decoupled counterparts have been lost in the fully random structures, concluding that geometrical randomness, specifically positions randomness, is the most dominant parameter characterising wave propagation and controlling stop/pass band behaviour.

Acknowledgements This work was supported by International Graduate Education Scholarship (YLSY) programme funded by The Ministry of National Education of Türkiye.

Author contribution Sinan Eraslan contributed to conceptualization, methodology, software, formal analysis, writing—original draft, visualization, data curation Inna M. Gitman contributed to conceptualization, methodology, supervision, resources, writing—review & editing Harm Askes contributed to supervision, resources, writing—review & editing Rene de Borst contributed to supervision, writing—review & editing.

Funding Partial financial support was received by the first author from International Graduate Education Scholarship (YLSY) programme funded by The Ministry of National Education of Türkiye.

Availability of data and materials The raw/processed data required to reproduce these findings cannot be shared at this time as the data also forms part of an ongoing study.

Declarations

Conflict of interest The authors have no competing interests to declare that are relevant to the content of this article.

Ethical approval Not applicable.

Consent to participate Not applicable.

Consent for publication Not applicable.

References

1. Kushwaha, M., Halevi, P., Dobrzynski, L., Djafari-Rouhani, B.: Acoustic band structure of periodic elastic composites. Phys. Rev. Lett. **71**, 2022–2025 (1993). https://doi.org/10.1103/PhysRevLett.71.2022
2. Vasseur, J., Deymier, P., Chenni, B., Djafari-Rouhani, B., Dobrzynski, L., Prevost, D.: Experimental and theoretical evidence for the existence of absolute acoustic band gaps in two-dimensional solid phononic crystals. Phys. Rev. Lett. **86**, 3012–5 (2001). https://doi.org/10.1103/PhysRevLett.86.3012
3. Sigalas, M., Economou, E.: Band structure of elastic waves in two dimensional systems. Solid State Commun. **86**(3), 141–143 (1993). https://doi.org/10.1016/0038-1098(93)90888-T
4. Wu, T., Wu, L., Huang, Z.: Frequency band-gap measurement of two-dimensional air/silicon phononic crystals using layered slanted finger interdigital transducers. J. Appl. Phys. **97**(9), 094–916 (2005). https://doi.org/10.1063/1.1893209
5. Song, Y., Gitman, I., Parnell, W., Askes, H.: The influence of random microstructure on wave propagation through heterogeneous media. Int. J. Fract. (2017). https://doi.org/10.1007/s10704-016-0170-2
6. Wang, Y., Li, F.M., Kishimoto, K., Wang, Y.S., Huang, W.: Elastic wave band gaps in magnetoelectroelastic phononic crystals. Wave Motion **46**(1), 47–56 (2009). https://doi.org/10.1016/j.wavemoti.2008.08.001
7. Hsu, J., Wu, T.: Efficient formulation for band-structure calculations of two-dimensional phononic-crystal plates. Phys. Rev. (2006). https://doi.org/10.1103/PhysRevB.74.144303
8. Lan, M., Wei, P.: Band gap of piezoelectric/piezomagnetic phononic crystal with graded interlayer. Acta Mechanica (2014). https://doi.org/10.1007/s00707-013-0984-1
9. Ding, R., Su, X., Zhang, J., Gao, Y.: Tunability of longitudinal wave band gaps in one dimensional phononic crystal with magnetostrictive material. J. Appl. Phys. **115**(7), 074–104 (2014). https://doi.org/10.1063/1.4866364
10. Bou Matar, O., Robillard, J., Vasseur, J., Hladky-Hennion, A., Deymier, P., Pernod, P., Preobrazhensky, V.: Band gap tunability of magneto-elastic phononic crystal. J. Appl. Phys. (2012). https://doi.org/10.1063/1.3687928
11. Zhou, C., Sai, Y., Chen, J.: Tunable lamb wave band gaps in two-dimensional magnetoelastic phononic crystal slabs by an applied external magnetostatic field. Ultrasonics **71**, 69–74 (2016). https://doi.org/10.1016/j.ultras.2016.05.023
12. Vasseur, J.O., Matar, O.B., Robillard, J.F., Hladky-Hennion, A.C., Deymier, P.A.: Band structures tunability of bulk 2d phononic crystals made of magneto-elastic materials. AIP Adv. **1**(4), 041–904 (2011). https://doi.org/10.1063/1.3676172
13. Baumgartl, J., Zvyagolskaya, M., Bechinger, C.: Tailoring of phononic band structures in colloidal crystals. Phys. Rev. Lett. **99**, 205–503 (2007). https://doi.org/10.1103/PhysRevLett.99.205503
14. Zhang, S., Shi, Y., Gao, Y.: A mechanical-magneto-thermal model for the tunability of band gaps of epoxy/terfenol-d phononic crystals. J. Appl. Phys. (2015). https://doi.org/10.1063/1.4926483
15. Zhang, G., Gao, Y.: Tunability of band gaps in two-dimensional phononic crystals with magnetorheological and electrorheological composites. Acta Mech. Solida Sin. **34**, 1–13 (2020). https://doi.org/10.1007/s10338-020-00189-6
16. Robillard, J., Bou Matar, O., Vasseur, J., Deymier, P., Stippinger, M., Hladky-Hennion, A., Pennec, Y., Djafari-Rouhani, B.: Tunable magnetoelastic phononic crystals. Appl. Phys. Lett. (2009). https://doi.org/10.1063/1.3236537
17. Wang, Y., Li, F., Huang, W., Jiang, X., Wang, Y., Kishimoto, K.: Wave band gaps in two-dimensional piezoelectric/piezomagnetic phononic crystals. Int. J. Solids Struct. **45**(14), 4203–4210 (2008). https://doi.org/10.1016/j.ijsolstr.2008.03.001
18. Claeyssen, F., Lhermet, N., Barillot, F., Letty, R.: Giant dynamic strains in magnetostrictive actuators and transducers (2006)
19. Eraslan, S., Gitman, I.M., Askes, H., de Borst, R.: Determination of representative volume element size for a magnetorheological elastomer. Comput. Mater. Sci. **203**, 111–070 (2022). https://doi.org/10.1016/j.commatsci.2021.111070
20. Xu, M., Gitman, I.M., Askes, H.: A gradient-enriched continuum model for magneto-elastic coupling: formulation, finite element implementation and in-plane problems. Comput. Struct. **212**, 275–288 (2019). https://doi.org/10.1016/j.compstruc.2018.11.004
21. Pang, Y., Liu, J., Wang, Y., Fang, D.: Wave propagation in piezoelectric/piezomagnetic layered periodic composites. Acta Mech. Solida Sin. **21**, 483–490 (2008). https://doi.org/10.1007/s10338-008-0858-6
22. Mane H.: Mathematical modeling and numerical simulation of magnetoelastic coupling. Doctoral thesis, Technische Universität Kaiserslautern (2019)
23. Song, Y.: The influence of random microstructure on wave propagation through heterogeneous media. Doctoral thesis, The University of Sheffield (2015)

24. Wang, Y.Z., Li, F.M., Huang, W.H., Jiang, X., Wang, Y.S., Kishimoto, K.: Wave band gaps in two-dimensional piezoelectric/piezomagnetic phononic crystals. Int. J. Solids Struct. **45**, 4203–4210 (2008). https://doi.org/10.1016/j.ijsolstr.2008.03.001
25. Gitman, I.M., Song, Y.: Fibonacci sequence for modelling stop bands in random microstructure. ZAMM J. Appl. Math. Mech./Zeitschrift für Angewandte Mathematik und Mechanik **98**, 270–276 (2018). https://doi.org/10.1002/zamm.201700010
26. Mech, R., Kaleta, K.: Influence of Terfenol-D powder volume fraction in epoxy matirx composites on their magnetomechanical properies. Acta Mechanica et Automatica **11**(3), 233–236 (2017). https://doi.org/10.1515/ama-2017-0036